ACS APPLIED MATERIALS & INTERFACES

Research Article

www.acsami.org

O-(Carboxymethyl)-chitosan Nanofiltration Membrane Surface Functionalized with Graphene Oxide Nanosheets for Enhanced Desalting Properties

Jiali Wang,[†,‡] Xueli Gao,*[,†,‡] Jian Wang,[†,‡] Yi Wei,[†,‡] Zhaokui Li,[§] and Congjie Gao[†,‡]

[†]Key Laboratory of Marine Chemistry Theory and Technology, Ministry of Education and [‡]College of Chemistry and Chemical Engineering, Ocean University of China, Qingdao 266100, China

[§]The Institute of Seawater Desalination and Multipurpose Utilization, State Oceanic Administration, Tianjin 300192, China

Supporting Information

ABSTRACT: A novel *O*-(carboxymethyl)-chitosan (OCMC) nanofiltration (NF) membrane is developed via surface functionalization with graphene oxide (GO) nanosheets to enhance desalting properties. Using ring-opening polymerization between epoxy groups of GO nanosheets and amino groups of OCMC active layer, GO nanosheets are irreversibly bound to the membrane. The OCMC NF membranes surface-functionalized with GO nanosheets are characterized by Fourier-transform infrared spectroscopy, X-ray photoelectron spectroscopy, scanning electron microscopy, atomic force microscopy, contact angle analyzer, and zeta potential analyzer. The membranes exhibit not only higher permeability but also better salt rejections than the pristine membranes and the commercial NF membranes; besides, the desalting properties are enhanced with the concentration of GO nanosheets increasing. Furthermore, the transport mechanism of GO−OCMC NF membranes reveals that the nanoporous structure of GO−OCMC functional layer and size exclusion and electrostatic repulsion of water nanochannels formed by GO nanosheets lead to the membranes possessing enhanced desalting properties.

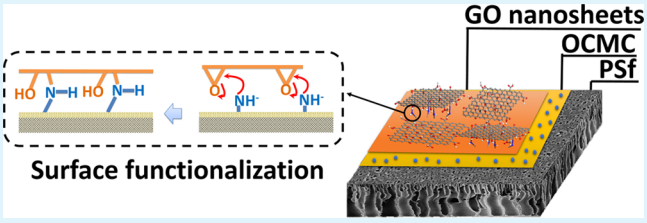

KEYWORDS: *graphene oxide, O-(carboxymethyl)-chitosan, nanofiltration membrane, surface functionalization, desalination*

1. INTRODUCTION

Water shortage is a worldwide problem due to dwindling water resources and increasing water consumption. Desalination using nanofiltration (NF) membranes is nowadays an appropriate choice for brackish and seawater treatment.[1−5] NF membranes with high retention of multivalent anion salts, low operational pressure, and high water flux can considerately reduce the investment and energy costs of separation processes. Thus, it is of great interest to develop novel NF membranes assuring high salt rejections, as well as high water permeability.

Graphene (GN) is a two-dimensional sheet of sp^2-bonded carbon atoms in a hexagonal honeycomb lattice with atomic thickness and high mechanical strength.[6] Attractive advantages of GN over membranes enable faster water transport, low-pressure requirements, and a wider range of operating conditions than previously possible.[7] Graphene oxide (GO) nanosheets are the highly oxidized form of GN with carboxyl, epoxy, and hydroxyl groups in the plane and the edges.[8] These oxygen-containing functional groups endow GO nanosheets with good hydrophilicity and provide possibilities for the reactions with amino groups.[9,10] On the basis of its good hydrophilicity and chemical properties, GO nanosheets possess promising potentials for water purification.[11,12]

O-(carboxymethyl)-chitosan (OCMC) is a derivative of the naturally occurring polysaccharide chitosan (CS) with both primary amino and hydroxyl groups.[13] It can be employed as the material of the active layers to prepare NF membranes through methods of surface cross-linking,[14] blending,[15] ultraviolet irradiation,[16] surface functionalization,[17] etc.

Recently, GO nanosheets as a novel nanomaterial have been used for membrane fabrication via phase inversion, layer-by-layer deposition, and surface functionalization to improve antifouling properties, permeability, and mechanical strength of membranes.[18−24] Although GO membranes prepared by phase-inversion method have relatively improved antifouling performances, the majority of GO nanosheets is embedded in the bulk of the membrane, rendering it unavailable to form a functional layer on the membrane surface. The approach of layer-by-layer deposition has partly enhanced separating properties of GO membranes, but GO nanosheets with free surface π electrons on the basal plane tend to stack up on the membrane surface due to the $\pi-\pi$ conjugate interaction.[25] The aggregation of GO nanosheets could further hamper the surface-based water transport of membranes, rendering the degradation of membrane separating performances. Additionally, some studies have focused on surface functionalization. While it has

Received: December 17, 2014
Accepted: January 30, 2015
Published: January 30, 2015

DOI: 10.1021/am508903g
ACS Appl. Mater. Interfaces 2015, 7, 4381−4389

Scheme 1. Procedure to Synthesize OCMC NF Membranes Surface-Functionalized with GO Nanosheets

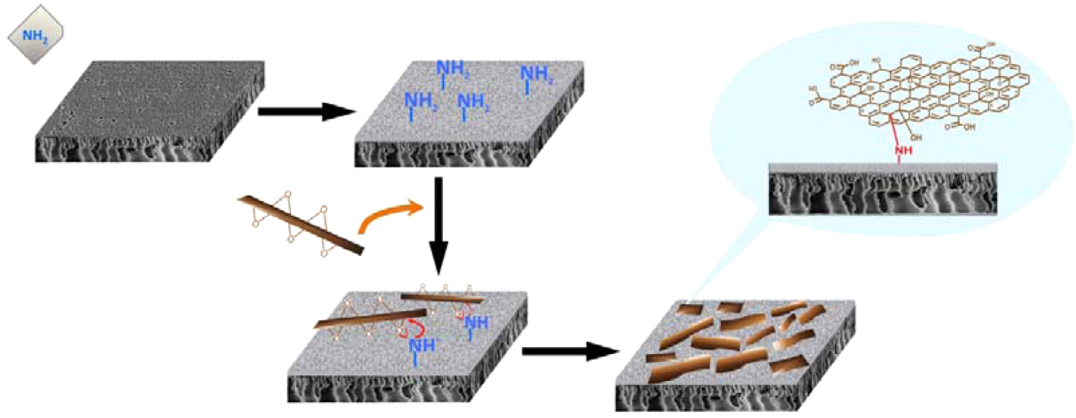

effectively enhanced the antimicrobial properties of GO membranes, the generated amide and ester groups have the tendency of hydrolysis, leading to the inactivation of the functional layer. To solve these problems, GO nanosheets should be covalently and irreversibly bonded on the membrane surface without aggregation to improve separating properties. Surface functionalization is a feasible approach to change the surface properties of membranes in a defined selective way while preserving its porous structure. Using ring-opening polymerization between epoxy groups in GO nanosheets and amino groups in the OCMC active layer, GO nanosheets can be irreversibly bound to the membrane surface. Furthermore, the mass-transport process through GO−OCMC NF membranes is explored for the first time. To date, surface functionalization of the OCMC membranes with GO nanosheets that enhances desalting properties has not been investigated.

In this paper, we report a novel OCMC NF membrane surface functionalized with GO nanosheets to enhance desalting properties. GO nanosheets are covalently bound to the OCMC active layer of membranes, yielding both higher permeability and better separating property, compared with the pristine membrane and the commercial NF membranes. Moreover, the concentration of GO nanosheets has a remarkable influence on the morphology and separating performances of membranes, including hydrophilicity, surface roughness, water flux, and salt rejection. We also explore the mechanism of separation and permeation for OCMC NF membranes surface functionalized with GO nanosheets.

2. EXPERIMENTAL SECTION

2.1. Materials. The following chemicals were used as received: *O*-(carboxymethyl)-chitosan (OCMC, 80 wt % of deacetylation, Dibo), graphite (GN, Fada), H_2SO_4 (95 wt %, Sinopharm), $KMnO_4$ (Sinopharm), H_2O_2 (30 wt %, Sinopharm), HCl (36−38 wt %, Sinopharm), Epichlorohydrin (ECH, Basf), NaOH (Sinopharm), NaCl (Sinopharm), Na_2SO_4 (Sinopharm), and KCl (Sinopharm). The commercial membrane of polysulfone (PSf, Lanjing) was used as supporting layer, and NTR 7450 (Hydranautics/Nitto Denko), NF 200 and NF 270 (Dow Deutschland), DK (GE Osmonics), OPMN-K (Vladipor), and NF-PES-10 (Microdyne Nadir Filtration) were used for comparison test.

2.2. Methods. *2.2.1. Preparation of GO Nanosheets.* There are many methods in practice for the preparation of GO nanosheets.[26−29] In this experiment, a modified Hummer's method was used to prepare GO nanosheets from natural graphite powder.[26] First, flake graphite was oxidized in a mixture of concentrated H_2SO_4 and $KMnO_4$ below 10 °C. Then, the temperature of mixture was maintained at 30−40 °C for 30 min. Second, the resulting pasty solution was diluted, and the temperature was maintained at 90−100 °C for 15−20 min. Third, hydrogen peroxide was added, and the color of the suspension changed from brown to yellowish brown. Finally, GO was obtained by centrifugation and ultrasonication in water. After drying the residue in vacuum drying oven, GO nanosheets were used for the further characterization and membrane preparation.

2.2.2. Preparation of OCMC NF Membranes Surface-Functionalized with GO Nanosheets. The overall membrane synthesis procedure is illustrated in Scheme 1. First, the filtered and degassed 1.7 wt % of OCMC aqueous solution was coated on the PSf membrane by a finely polished glass rod. This membrane was then dried in a convection oven at 60 °C for 1 h, and the OCMC-coating was formed on the PSf membrane support. Second, the OCMC-coated membrane was soaked in the GO nanosheets solution that was composed of GO nanosheets (0, 2, 10, 100 mg/L) and ECH (2 wt %) in ethanol at pH ≈ 14 and was maintained in a convection oven at 50 °C for 3 h. ECH was cross-linked with OCMC-coating, while the epoxy groups in GO nanosheets were covalently bonded to amino groups in OCMC-coated membrane via surface functionalization. Finally, the membranes were rinsed thoroughly with ethanol to remove excessive GO and ECH. The membranes were stored in deionized water for further characterization.

2.3. Characterization. The Fourier-transform infrared (FTIR) spectroscopy was performed using Tensor 27 spectrometer (Bruker, Germany) in the range of 4000−400 cm^{-1} at room temperature. X-ray powder diffraction (XRD) patterns were recorded using D8 ADVANCE diffractometer (Bruker, Germany), equipped with a Cu Kα radiation source (λ= 1.5418 Å). Raman scattering was performed on NEXUS 670 Microscopy (Thermo Nicolet, USA) with an excitation laser of 532 nm. The X-ray photoelectron spectroscopy (XPS) measurement was performed on ESCALAB 250 spectrophotometer (Thermo Fisher SCIENTIFIC, USA) with an achromatic Mg/Al X-ray source at 450W. Scanning electron microscopy (SEM) was observed using S-4800 scanning electron microscope (Hitachi, Japan) at a 15 kV accelerating voltage. The samples were coated with gold under an argon purge before the characterization. Atomic force microscopy (AFM) images were recorded using Multimode-V microscope (Veeco, USA) in contact mode. Contact angle measurements were performed with a DSA100 contact angle analyzer (Kruss, Germany) using a sessile drop technique. At least two replicates were used, and ∼20 Milli-Q water drops per replicate were delivered for calculation of the average value of the contact angle. Membrane zeta potentials were measured using a NANOPLUS zeta potential analyzer (Micromeritics, USA) with KCl electrolyte solution. The zeta potentials were measured over the range of pH 3−10. Results shown for each pH are an average of six measurements taken at that pH.

2.4. Membrane Permeation Measurements. NF membrane Performance Evaluation Instrument (Hangzhou Water Treatment Center) was used to evaluate water flux and salt rejection of

DOI: 10.1021/am508903g
ACS Appl. Mater. Interfaces 2015, 7, 4381−4389

membranes via cross-flow filtration. Prior to filtration, the membranes were wetted by pressurization at 2 MPa for 30 min. The pure water flux was measured (P = 0.25, 0.5, 1.0, and 1.5 MPa, t = 25 °C, v = 5.0 m/s). NaCl solution (1000 mg/L) as a representative monovalent salt solution and Na_2SO_4 solution (1000 mg/L) as a representative divalent salt solution were used for the single salt filtration, respectively. The permeate flux and salt rejection were measured (P = 0.25, 0.5, 1.0, and 1.5 MPa, t = 25 °C, v = 5.0 m/s). The concentration of the feed solution and the raw solution were measured by conductivity meter (DDS-307A, Leici, China)

For all the tested salt solutions and natural water, the natural pH of 6.0 ± 0.1 was used. The average data were determined from three pieces of the membrane tested.

The flux was defined as the amount of permeate produced per unit area of membrane surface per unit time:

$$F = \frac{\Delta V}{A \cdot \Delta t} \tag{1}$$

where F is the flux ($L \cdot m^{-2} \cdot h^{-1}$); ΔV is the volume of product water (L); A is the area of membrane surface (m^2); Δt is the time of permeation (h).

The salt rejection was calculated by changing the ratio of electrical conductivity:

$$R = \left(1 - \frac{\kappa_1}{\kappa_0}\right) \times 100\% \tag{2}$$

where κ_0 is the feed conductivity (μS/cm); κ_1 the permeate conductivity (μS/cm).

2.5. Membrane Comparison Tests. The NF membranes studied were NTR 7450, NF 200, NF 270, DK, OPMN-K, NF-PES-10, and GO−OCMC membranes (100 mg/L GO nanosheets) for desalting performances. The membrane comparison tests were operated using NF membrane Performance Evaluation Instrument as mentioned above at 25 °C and 1 MPa, with the feed concentration of 1 g/L NaCl or 1 g/L Na_2SO_4 solution, respectively, and the permeate flux and salt rejection were measured. Prior to the experiments, all virgin NF membranes were soaked overnight in Milli-Q water.

3. RESULTS AND DISCUSSION

3.1. Characterization of OCMC NF Membranes Surface-Functionalized with GO Nanosheets. Figure 1 shows

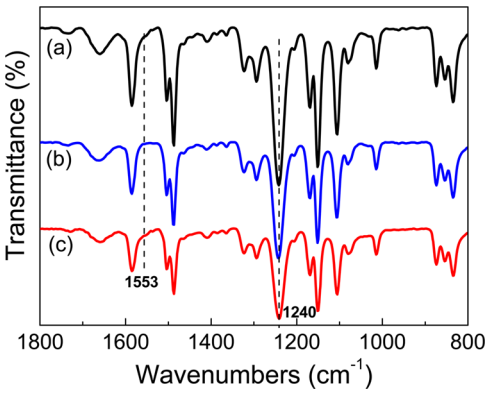

Figure 1. FTIR spectra of (a) OCMC/PSf membranes, (b) ECH−OCMC/PSf membranes, and (c) GO−OCMC/PSf membranes.

FTIR spectra of OCMC/PSf membranes, ECH−OCMC/PSf membranes, and GO−OCMC/PSf membranes. For OCMC/PSf membranes, as shown in Figure 1a, the peaks at 1555 and 1240 cm^{-1} are corresponding to −NH− bending vibration of $-NH_2$ and −OH bending vibrations, respectively. For ECH−OCMC/PSf membranes, the peak of $-NH_2$ stretching (1555 cm^{-1}) disappears, and the intensity of −OH stretching (1240 cm^{-1}) is increased (Figure 1b), as a consequence of the cross-linking between ECH and OCMC.[30] In GO−OCMC/PSf membranes, as shown in Figure 1c, the intensity of $-NH_2$ stretching (1550 cm^{-1}) becomes slightly stronger, while that of −OH stretching (1240 cm^{-1}) is much stronger than in ECH−OCMC/PSf membranes due to surface functionalization of GO nanosheets, which is consistent with the XPS data (Supporting Information, Figure S6). We can further demonstrate the surface binding of GO nanosheets by computing the cross-linking degree of ECH and OCMC from the ATR-FTIR spectra as shown according to the following equations:[31,32]

$$R_{NH_2} = \frac{I_{NH_2}}{I_{sulfone}}, \; R_{OH} = \frac{I_{OH}}{I_{sulfone}} \tag{3}$$

where I_{NH_2} and I_{OH} is the absorbance at 1555 and 1240 cm^{-1}, corresponding to the hydroxyl groups and primary amine, respectively, and $I_{sulfone}$ is the absorbance of PES at 1150 cm^{-1}. As shown in Table 1, R_{NH_2} is ordered as follows: OCMC/PSf membrane > GO−OCMC/PSf membrane > ECH−OCMC/PSf membrane, and R_{OH} is ordered as follows: GO−OCMC/PSf membrane > ECH−OCMC/PSf membrane > OCMC/PSf membrane. Therefore, GO nanosheets are covalently bonded to OCMC NF membranes, whereas the cross-linking degree of ECH in GO−OCMC/PSf membranes is lower than that in ECH−OCMC/PSf membranes. It implies that GO nanosheets hindered the cross-linking reaction of ECH and OCMC, resulting in the lower cross-linking degree of GO−OCMC/PSf membranes. GO nanosheets possibly blocked the penetration of ECH into OCMC coating due to the sheet-like structure. Surface functionalization with GO nanosheets is thus successful in fabricating GO−OCMC/PSf membranes.

Table 1. R_{NH_2} and R_{OH} of OCMC/PSf, EHC-OCMC/PSf, and GO−OCMC/PSf Membranes

	OCMC/PSf membranes	ECH−OCMC/PSf membranes	GO−OCMC/PSf membranes
R_{NH_2}	0.1208	0.0184	0.1024
R_{OH}	1.137	1.1632	1.3887

The surface morphology of ECH−OCMC/PSf and GO−OCMC/PSf membranes are visualized by SEM, and the results are shown in Figure 2. In Figure 2a, the surface of ECH−OCMC/PSf membranes is not completely smooth with some nodules and pores of similar sizes, which comes from the homogeneous cross-linking reaction of ECH and OCMC. After surface functionalized with GO nanosheets, as shown in Figure 2b, the morphology of GO−OCMC/PSf membranes is significantly changed, where pore sizes and nodules are reduced on the surface. As the concentration of GO nanosheets increases, pores and nodules become invisible, and the membrane surface is composed of tight and smooth structures with slits observed in Figure 2b−d.

Figure 3 shows the three-dimensional (3D) AFM surface images of ECH−OCMC/PSf and GO−OCMC/PSf membranes. The data of the surface roughness are presented in Table 2. Generally, the surface roughness is an important parameter correlating with membrane antifouling property and local mass transfer.[33] The surface of ECH−OCMC/PSf membrane presents high roughness with several obvious "peaks" and "valleys" in Figure 3a. After surface functionalized with GO nanosheets, the fluctuations are replaced by numerous

DOI: 10.1021/am508903g
ACS Appl. Mater. Interfaces 2015, 7, 4381−4389

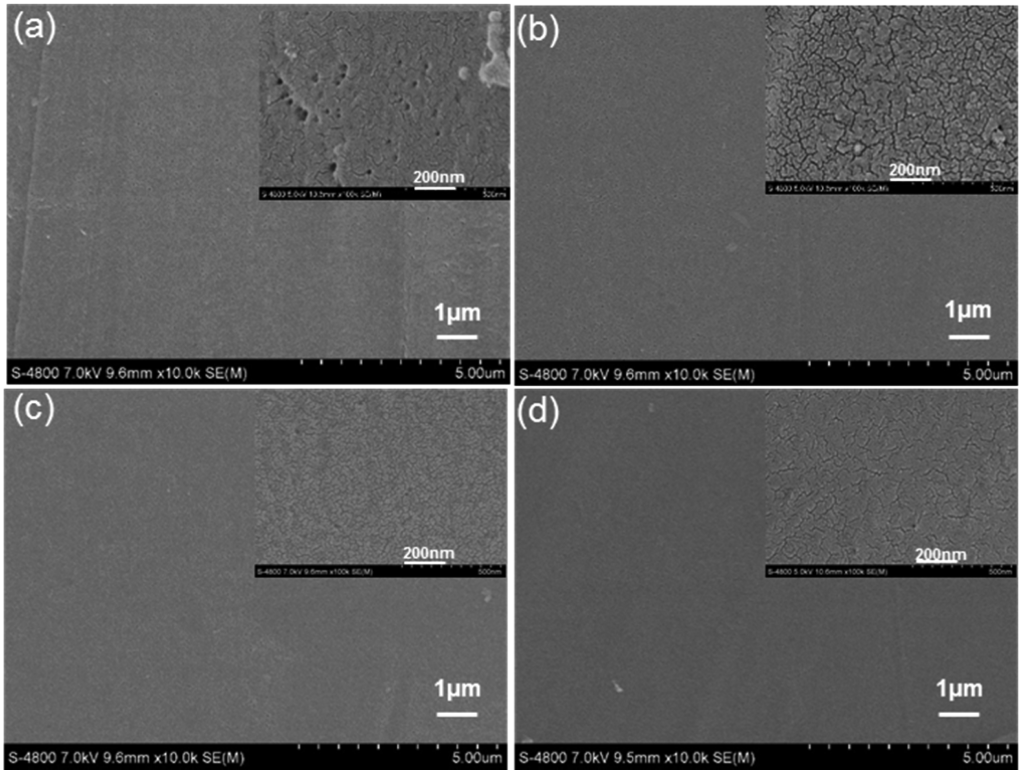

Figure 2. SEM images of (a) ECH−OCMC/PSf membranes and (b−d) GO−OCMC/PSf membranes with GO nanosheets (2, 10, 100 mg/L).

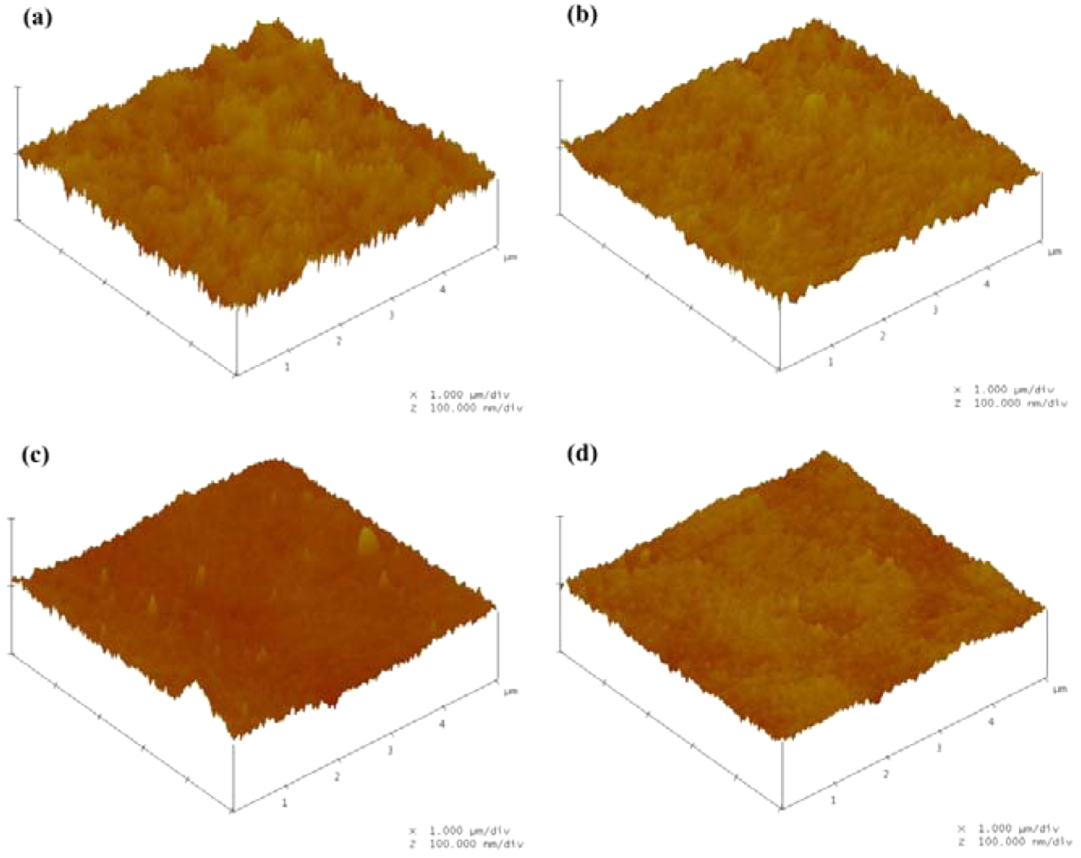

Figure 3. AFM 3D images of (a) ECH−OCMC/PSf membranes and (b−d) GO−OCMC/PSf membranes with GO nanosheets (2, 10, 100 mg/L).

small ones, which leads to a smoother surface on GO−OCMC/PSf membrane. The root-mean square roughness (RMS) decreases from 8.211 to 4.149 nm with increasing the GO nanosheets concentration from 0 to 100 mg/L, shown in Table

DOI: 10.1021/am508903g
ACS Appl. Mater. Interfaces 2015, 7, 4381−4389

Table 2. Surface Roughness of Membranes

membranes	RMS[a] (nm)
ECH−OCMC/PSf membrane	8.21 ± 0.264
GO−OCMC/PSf membrane (2 mg/L GO nanosheets)	5.91 ± 0.204
GO−OCMC/PSf membrane (10 mg/L GO nanosheets)	5.48 ± 0.190
GO−OCMC/PSf membrane (100 mg/L GO nanosheets)	4.18 ± 0.112

[a]Means of three samples for each membrane.

2. It suggests that the decrease in RMS values is attributed to the surface functionalization of GO nanosheets. For ECH−OCMC/PSf membranes, OCMC usually has a tendency of instantaneous demixing, leading to a high RMS value and a reduction in uniformity. After surface functionalization, GO nanosheets are covalently bounded to the surface of OCMC active layer, reducing the swelling of OCMC, so that surface roughness of GO−OCMC membranes decreases. In addition, the increasing concentration of GO nanosheets could provide more GO nanosheets in large sizes. It could cover a wide area that exceeds the area of voids between the sheets and yields the most compact and smooth membrane surface.[34,35]

Surface hydrophilicity is one of the most important factors in determining permeation and antifouling properties of membranes.[36] Water static contact angle (WSCA) of the membrane surface is measured to characterize surface hydrophilicity, and the results are shown in Figure 4; WSCA decreases from 62° to

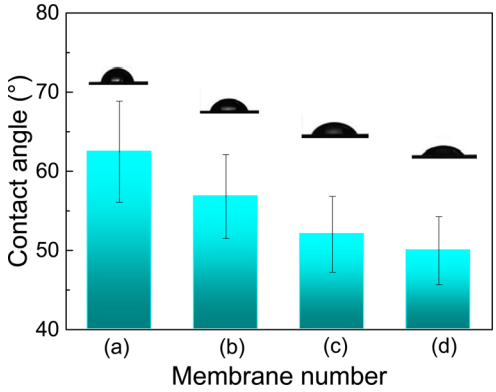

Figure 4. Water static contact angle of (a) ECH−OCMC/PSf membranes and (b−d) GO−OCMC/PSf membranes with GO nanosheets (2, 10, 100 mg/L).

49.8° with the increasing concentration of GO nanosheets solution from 0 to 100 mg/L. It indicates that the surface functionalization of GO nanosheets effectively enhances the hydrophilicity of membranes. In previous reports, GO nanosheets have good hydrophilicity due to plenty of carboxyl, epoxy, and hydroxyl groups.[37] Surface binding of GO nanosheets endows OCMC NF membrane with high hydrophilicity. Thus, GO−OCMC/PSf membranes present higher hydrophilicity, which could benefit water permeability of membranes.

The results of the zeta potential versus pH for the membranes are shown in Figure 5. The ECH−OCMC and GO−OCMC membranes are all positively charged at low pH with an isoelectric point between pH 3−6 and negatively charged at high pH. The isoelectric point of ECH−OCMC is 5.3, which is consistent with previously reports.[38] More specifically, the isoelectric points of GO−OCMC membranes (2, 10, 100 mg/L) are 4.4, 4.2 and 4.1, respectively. GO−

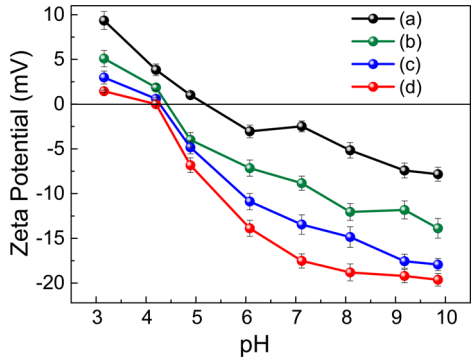

Figure 5. Zeta potential measurements of (a) ECH−OCMC/PSf membranes and (b−d) GO−OCMC/PSf membranes with GO nanosheets (2, 10, 100 mg/L) at various pH.

OCMC membranes are more negative than ECH−OCMC membranes. When the concentration of GO is 100 mg/L, the GO−OCMC membranes attain more negative zeta potential (ca. −20 mV at pH 9.8) than ECH−OCMC (ca. −8 mV at pH 9.8). Zeta potential curves of this shape are characteristic of surfaces with both acidic and basic functional groups. With increasing GO concentration, the charges of the GO−OCMC membrane surface relatively decrease. Note that GO nanosheets are negatively charged due to the aromatic matrix and oxygen-containing functional groups.[8−10] The attachment of GO nanosheets significantly contributes to the surface charges of membranes. Since GO nanosheets are increasingly introduced on the membrane surface, the density of functional groups and the charge density increase, resulting in the more negative GO−OCMC membrane surfaces. Therefore, the effective membrane charge could be attributed to the inherent charges due to protonation and dissociation of surface carboxyl and hydroxyl groups.

3.2. Membrane Permeation. Figure 6 shows the resultant pure water fluxes of ECH−OCMC/PSf and GO−OCMC/PSf

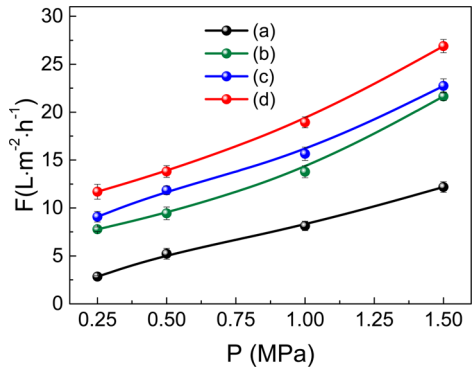

Figure 6. Pure water fluxes of (a) ECH−OCMC/PSf membranes and (b−d) GO−OCMC/PSf membranes with GO nanosheets (2, 10, 100 mg/L).

membranes. The pure water fluxes of membranes significantly increase as GO nanosheets concentration increases. When the concentration of GO nanosheets is 100 mg/L, the GO−OCMC/PSf membrane has a maximum pure water flux of 26.89 $L \cdot m^{-2} \cdot h^{-1}$ at 1.5 MPa, which is about twice that of the ECH−OCMC/PSf membrane. The increase of water flux could be attributed to the increase of hydrophilicity of GO−OCMC functional layer and the decrease of permeability resistance. On

DOI: 10.1021/am508903g
ACS Appl. Mater. Interfaces 2015, 7, 4381−4389

one hand, GO nanosheets, which possess a great amount of hydrophilic groups, promote the interaction between membrane surface and water molecules. On the other hand, GO naonosheets can cover a wide area without exposing the underlying polymer layer.[34] Consequently, GO naonosheets would hinder the cross-linking between ECH and OCMC due to the unique sheet-like structure, rendering the decrease of permeability resistance from the cross-linking network. GO–OCMC/PSf membranes thus exhibited the increase of the permeate flux.

The separation performance of ECH–OCMC/PSf and GO–OCMC/PSf membranes is examined using NaCl as a representative monovalent salt and Na_2SO_4 as a representative divalent salt, and the results are shown in Figures 7 and 8. GO–

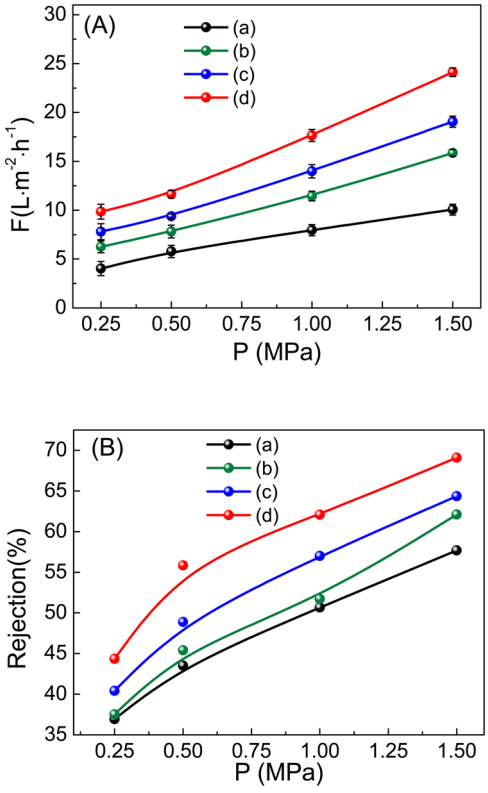

Figure 7. (A) Permeation flux and (B) NaCl rejection of (a) ECH–OCMC/PSf membranes and (b–d) GO–OCMC/PSf membranes with GO nanosheets (2, 10, 100 mg/L).

OCMC/PSf membranes and ECH–OCMC/PSf membranes both have the higher rejection of Na_2SO_4 over NaCl solution. Previous study presented that the permeation flux of Na_2SO_4 and NaCl both had similar flux of ~18 $L·m^{-2}·h^{-1}$ for ECH–OCMC/PS membranes.[30] In this paper, GO nanosheets were introduced into the OCMC NF membrane via surface modification. Therefore, GO–OCMC/PSf membranes and ECH–OCMC/PSf membranes display almost similar range of flux rate for both Na_2SO_4 and NaCl solution. Permeation flux and salt rejection of GO–OCMC/PSF membranes concurrently increase with the additive GO nanosheets increasing. When the concentration of GO nanosheets is 100 mg/L, GO–OCMC/PSf membranes achieve the maximum salt rejections of 69.10% and 93.74% for a feed NaCl and Na_2SO_4 concentration of 1000 mg/L, respectively, and the corresponding permeation fluxes of 24.12 and 24.07 $L·m^{-2}·h^{-1}$ at 1.5 MPa.

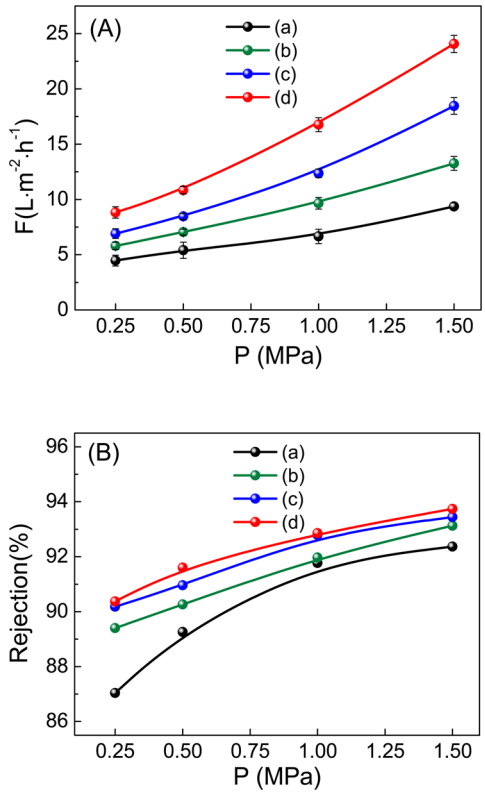

Figure 8. (A) Permeation flux and (B) Na_2SO_4 rejection of (a) ECH–OCMC/PSf membranes and (b–d) GO–OCMC/PSf membranes with GO nanosheets (2, 10, 100 mg/L).

This indicates that GO nanosheets effectively enhance the permeability and salt rejection of GO–OCMC/PSf membranes. On one hand, the increase of hydrophilicity of GO–OCMC functional layer and the decrease of permeability resistance attributed to the increase of permeation flux, as shown above. On the other hand, the presence of multiple functional groups on GO naonsheets resulted in a negative surface charge distribution on membrane surface and nanoscale interlayer spacing of GO nanosheets resulted in size exclusion in the GO–OCMC functional layer, which could effectively hinder the passage of salt ions for GO–OCMC/PSf membranes. Moreover, the higher retention for Na_2SO_4 than NaCl is in accordance to the diffusion coefficients between the salts. According to previous studies, the order of the diffusion coefficients is inversely reflected in the retention sequence.[39,40] As the diffusion coefficient for Na_2SO_4 is much lower than for NaCl, for Na_2SO_4 a low diffusion contribution can be expected resulting in a higher retention. Thus, GO–OCMC/PSf membranes present both higher water permeation and higher salt rejection than ECH–OCMC/PSf membrane.

3.3. Comparison of Commercial NF Membranes in Desalting Properties. In Figure 9, the GO–OCMC membranes are compared with the commercial NF membranes for desalting properties. The comparison focuses on two quantities of interest: the permeation flux through the membranes and salt rejections. The separation results show that the GO–OCMC NF membranes possess better desalting properties than commercial NF membranes. The permeation flux of NaCl is nearly 2–15 times higher in GO–OCMC NF membrane than it is in other types of NF membranes, and the rejection is the maximum of 62%; while that of Na_2SO_4 is

DOI: 10.1021/am508903g
ACS Appl. Mater. Interfaces 2015, 7, 4381–4389

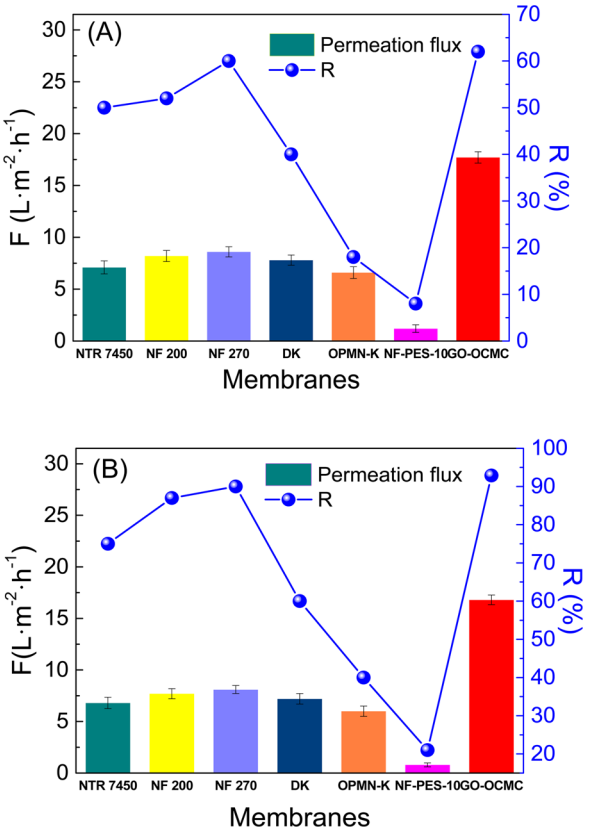

Figure 9. Comparison of NF membranes in (A) NaCl and (B) Na_2SO_4 permeation.

nearly 2−21 times higher, and the rejection is the maximum of 92.9%. Therefore, the GO−OCMC membranes show significant improvement in membrane desalting properties suited for large-scale industrial applications.

3.4. Transport and Separation Mechanism. To further illustrate the transport and separation mechanism of GO−OCMC/PSF membranes, the simulation diagram is shown in Figure 10. Previous study found that the self-assembled GO

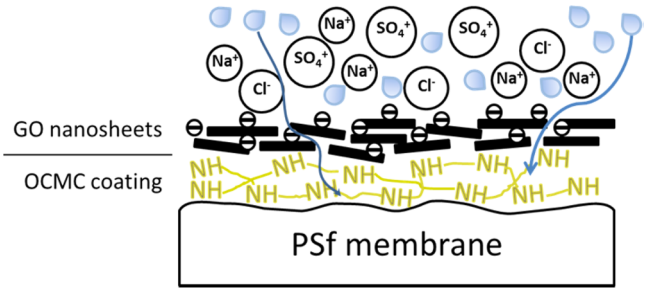

Figure 10. Schematic of the separating process of GO−OCMC/PSf membranes.

layer is composed of 2−3 GO nanosheets.[34,41] In our research, we assumed that the top layer of the membrane contains 2−3 GO nanosheets. The interlayer distance of single-layered GO nanosheets is 0.7−1 nm owing to multiple functional groups on the surface of GO platelets. When GO stacking, water nanochannels (~0.7−1 nm thick) between GO single sheets are formed.[42,43] Consequently, the GO−OCMC/PSF membrane surface consists of water nanochannels in the diameter of 0.7−1.0 nm.

Research on nanoporous GN menbranes suggests that single-layer GNs with the diameter of ~0.4 nm pores can reach water permeability as high as 2.75×10^3 $L \cdot m^{-2} \cdot h^{-1} \cdot MPa^{-1}$.[7] Owing to water nanochannels with hydrophilic groups, OH groups on the GO−OCMC/PSf membrane surface can hydrogen bond with water and offer a smoother entropic landscape for water molecules to traverse, thus allowing for faster overall water flow between GO nanosheets.[44] Therefore, GO nanosheets are supposed to scarcely influence the water flux of membranes. Moreover, GO naonosheets with good coverage capacity on OCMC coatings hindered the cross-linking between ECH and OCMC so that the cross-linking degree between ECH and OCMC decreased, endowing the functional layer of GO−OCMC/PSf membranes with higher permeability than that of ECH−OCMC/PSf membranes. When GO nanosheets increasingly distributed on GO−OCMC/PSf membranes, the reacting density of ECH and OCMC decreased, the reacting network decreased, and water passage tortuosity decreased. Permeation resistance of GO−OCMC/PSf membranes is thus weakened, allowing the increase of water flux.

In previous study, the decrease of cross-linking degree between ECH and OCMC usually resulted in the decrease of salt rejection.[30] However, our research presented both high water flux and high salt rejection. Electrostatic repulsion and size exclusion of the water nanochannel are the main factor for high salt rejection. The active layer of GO−OCMC/PSf membranes could acquire a negative surface charge distribution due to the ionization of carboxylic acid and hydroxyl groups of GO nanosheets in water,[36] which is consistent with the results of zeta potential. Electrostatic repulsion thus dominates the high salt retention. Moreover, the presence of functional groups on GO nanosheets resulted in 0.7−1 nm interlayer distance.[37] Size exclusion by GO nanosheets could also help GO−OCMC/PSf membranes effectively hinder the passage of salt ions. Therefore, water flux and salt rejection performances were greatly improved.

4. CONCLUSION

This paper has presented a feasible OCMC NF membrane preparation method via surface functionalization with GO nanosheets. GO nanosheets have effectively improved water flux and salt rejection of membranes. As the GO nanosheets concentration increases, GO−OCMC/PSf membranes have exhibited enhanced desalting properties including higher hydrophilicity, lower surface roughness, higher water fluxes, and higher salts rejections compared with other types of the commercial NF membranes. The good separation performance can be attributed to the nanoporous structure of functional layer, size exclusion, and electrostatic repulsion of water nanochannels on GO−OCMC NF membrane surface. In general, the OCMC NF membrane surface functionalized with GO nanosheets shows promise in water desalination due to high flux and good separation properties.

■ ASSOCIATED CONTENT

Supporting Information

XRD, Raman, FTIR, and XPS spectroscopy, and AFM of GO nanosheets and XPS of membranes. This material is available free of charge via the Internet at http://pubs.acs.org.

DOI: 10.1021/am508903g
ACS Appl. Mater. Interfaces 2015, 7, 4381−4389

AUTHOR INFORMATION

Corresponding Author

*Phone/Fax: +86-532-66782017. E-mail wangjialiouc@gmail.com or gxl_ouc@126.com.

Notes

The authors declare no competing financial interest.

ACKNOWLEDGMENTS

The authors gratefully acknowledge financial support from National Basic Research Program of China (Grant No. 2015CB655303), National Science & Technology Pillar Program during the 12th Five-year Plan Period (Grant No. 2015BAE06B03), and Marine Renewable Energy Project (Grant No. GHME2013JS07).

REFERENCES

(1) Chen, S.; Sun, G. High Sensitivity Ammonia Sensor Using a Hierarchical Polyaniline/Poly (Ethylene-co-Glycidyl Methacrylate) Nanofibrous Composite Membrane. *ACS Appl. Mater. Interfaces* **2013**, *5*, 6473−6477.

(2) Dun-Yen, K.; Henry, M. T.; Ji, Z.; Rudra, P. C.; David, S.; Haskell, W. B.; Christopher, W. J.; Sankar, N. Single-Walled Aluminosilicate Nanotube/Poly(vinyl alcohol) Nanocomposite Membranes. *ACS Appl. Mater. Interfaces* **2012**, *4*, 965−976.

(3) Roy Bernstein, E. A.; Ulbricht, M. UV-Photo Graft Functionalization of Polyethersulfone Membrane with Strong Polyelectrolyte Hydrogel and Its Application for Nanofiltration. *ACS Appl. Mater. Interfaces* **2012**, *4*, 3438−3446.

(4) Tai, M.; Gao, P.; Tan, B.; Sun, D.; Leckie, J. Highly Efficient and Flexible Electrospun Carbon-Silica Nanofibrous Membrane for Ultrafast Gravity-Driven Oil-Water Separation. *ACS Appl. Mater. Interfaces* **2014**, *6*, 9393−9401.

(5) Joris de Grooth, D. M. R.; Ploegmakers, Jeroen; Wiebe, M. V.; Kitty, N. Charged Micropollutant Removal with Hollow Fiber Nanofiltration Membranes Based On Polycation/Polyzwitterion/Polyanion Multilayers. *ACS Appl. Mater. Interfaces* **2014**, *6*, 933−938.

(6) Novoselov, K. S.; Geim, A. K.; Morozov, S. V.; Jiang, D.; Zhang, Y.; Dubonos, S. V.; Grigorieva, I. V.; Firsov, A. A. Electric Field Effect in Atomically Thin Carbon Films. *Science* **2004**, *306*, 666−669.

(7) Cohen-Tanugi, D.; Grossman, J. C. Water Desalination across Nanoporous Graphene. *Nano Lett.* **2012**, *12*, 3602−3608.

(8) Kai Feng, B. T.; Peiyi, W. Evaporating" Graphene Oxide Sheets (GOSs) for Rolled up GOSs and Its Applications in Proton Exchange Membrane Fuel Cell. *ACS Appl. Mater. Interfaces* **2013**, *5*, 832−836.

(9) Meng, F.; Zheng, S.; Li, H.; Liang, Q.; Liu, T. Formation of Ordered Nanostructures in Epoxy Thermosets: a Mechanism of Reaction-Induced Microphase Separation. *Macromolecules* **2006**, *39*, 5072−5080.

(10) Kyzas, G. Z.; Travlou, N. A.; Deliyanni, E. A. The Role of Chitosan as Nanofiller of Graphite Oxide for the Removal of Toxic Mercury Ions. *Colloids Surf., B* **2014**, *113*, 467−476.

(11) Dreyer, D. R.; Park, S.; Bielawski, C. W.; Ruoff, R. S. The Chemistry of Graphene Oxide. *Chem. Soc. Rev.* **2010**, *39*, 228−240.

(12) Dikin, D. A.; Stankovich, S.; Zimney, E. J.; Piner, R. D.; Dommett, G. H.; Evmenenko, G.; Nguyen, S. T.; Ruoff, R. S. Preparation and Characterization of Graphene Oxide Paper. *Nature* **2007**, *448*, 457−460.

(13) Osuji, G. O.; Cuero, R. G. Regulation of Ammonium Ion Salvage and Enhancement of the Storage Protein Contents of Corn, Sweet Potato, and Yam Tuber by N-(Carboxymethyl) Chitosan Application. *J. Agric. Food Chem.* **1992**, *40*, 724−734.

(14) Miao, J.; Chen, G. H.; Gao, C. J. A Novel Kind of Amphoteric Composite Nanofiltration Membrane Prepared from Sulfated Chitosan (SCS). *Desalination* **2005**, *181*, 173−183.

(15) Jegal, J.; Lee, K. H. Nanofiltration Membranes Based on Poly (Vinyl Alcohol) and Ionic Polymers. *J. Appl. Polym. Sci.* **1999**, *72*, 1755−1762.

(16) Tan, S.; Chen, Z. Preparation of Polyacrylonitrile Nanofiltration Membrane and Its Separation Property in the Treatment of Papermaking Effluent. *Trans. China Pulp Paper* **2002**, *17*, 63−66.

(17) Tangpasuthadol, V.; Pongchaisirikul, N.; Hoven, V. P. Surface Modification of Chitosan Films: Effects of Hydrophobicity on Protein Adsorption. *Carbohydr. Res.* **2003**, *338*, 937−942.

(18) Yu, L.; Zhang, Y.; Zhang, B.; Liu, J.; Zhang, H.; Song, C. Preparation and characterization of HPEI-GO/PES Ultrafiltration Membrane with Antifouling and Antibacterial Properties. *J. Membr. Sci.* **2013**, *447*, 452−462.

(19) Lee, J.; Chae, H. R.; Won, Y. J.; Lee, K.; Lee, C. H.; Lee, H. H.; Kim, I. C.; Lee, J. M. Graphene Oxide Nanoplatelets Composite Membrane with Hydrophilic and Antifouling Properties for Wastewater Treatment. *J. Membr. Sci.* **2013**, *448*, 223−230.

(20) Hu, M.; Mi, B. Enabling Graphene Oxide Nanosheets as Water Separation Membranes. *Environ. Sci. Technol.* **2013**, *47*, 3715−3723.

(21) Zhao, C.; Xu, X.; Chen, J.; Yang, F. Effect of Graphene Oxide Concentration on the Morphologies and Antifouling Properties of PVDF Ultrafiltration Membranes. *J. Environ. Chem. Eng.* **2013**, *1*, 349−354.

(22) Ganesh, B. M.; Isloor, A. M.; Ismail, A. F. Enhanced Hydrophilicity and Salt Rejection Study of Graphene Oxide-Polysulfone Mixed Matrix Membrane. *Desalination* **2013**, *313*, 199−207.

(23) Kang, H.; Gongping, L.; Yueyun, L.; Ziye, D.; Jie, S.; Wanqin, J. A Graphene Oxide Membrane with Highly Selective Molecular Separation of Aqueous Organic Solution. *Angew. Chem., Int. Ed.* **2014**, *53*, 1−5.

(24) Perreault, F.; Tousley, M. E.; Elimelech, M. Thin-Film Composite Polyamide Membranes Functionalized with Biocidal Graphene Oxide Nanosheets. *Environ. Sci. Technol. Lett.* **2013**, *12*, 233−239.

(25) Xu, Y.; Wu, Q.; Sun, Y.; Bai, H.; Shi, G. Three-dimensional Self-assembly of Graphene Oxide and DNA into Multifunctional Hydrogels. *ACS Nano* **2010**, *4*, 7358−7362.

(26) Titelman, G.; Gelman, V.; Bron, S.; Khalfin, R.; Cohen, Y.; Bianco-Peled, H. Characteristics and Microstructure of Aqueous Colloidal Dispersions of Graphite Oxide. *Carbon* **2005**, *43*, 641−649.

(27) Szabó, T.; Szeri, A.; Dékány, I. Composite Graphitic Nanolayers Prepared by Self-Assembly Between Finely Dispersed Graphite Oxide and A Cationic Polymer. *Carbon* **2005**, *43*, 87−94.

(28) Nakajima, T.; Matsuo, Y. Formation Process and Structure of Graphite Oxide. *Carbon* **1994**, *32*, 469−475.

(29) Hirata, M.; Gotou, T.; Horiuchi, S.; Fujiwara, M.; Ohba, M. Thin-film Particles of Graphite Oxide: High-Yield Synthesis and Flexibility of the Particles. *Carbon* **2004**, *42*, 2929−2937.

(30) Zhou, C.; Gao, X.l.; Li, S. S.; Gao, C. J. Fabrication and Characterization of Novel Composite Nanofiltration Membranes Based on Zwitterionic O-Carboxymethyl Chitosan. *Desalination* **2013**, *317*, 67−76.

(31) Wang, J.; Heng, S.; Gao, X.; Gao, C. Enhancing Antibiofouling Performance of Polysulfone (Psf) Membrane by Photo-Grafting of Capsaicin Derivative and Acrylic Acid. *Appl. Surf. Sci.* **2014**, *317*, 210−219.

(32) Gao, X. L.; Hui, W. J.; Wang, X.; Huang, C.; Gao, C. J. Surface-modified PSf UF Membrane by UV-assisted Graft Polymerization of Capsaicin Derivative Moiety for Fouling and Bacterial Resistance. *J. Membr. Sci.* **2013**, *445*, 146−155.

(33) Vrijenhoek, E. M.; Hong, S.; Elimelech, M. Influence of Membrane Surface Properties on Initial Rate of Colloidal Fouling of Reverse Osmosis and Nanofiltration Membranes. *J. Membr. Sci.* **2001**, *188*, 115−128.

(34) Yang, M.; Hou, Y.; Kotov, N. A. Graphene-based Multilayers: Critical Evaluation of Materials Assembly Techniques. *Nano Today* **2012**, *7*, 430−447.

(35) Kotov, N.; Magonov, S.; Tropsha, E. Layer-by-layer Self-Assembly of Alumosilicate-Polyelectrolyte Composites: Mechanism of Deposition, Crack Resistance, and Perspectives for Novel Membrane Materials. *Chem. Mater.* **1998**, *10*, 886−895.

DOI: 10.1021/am508903g
ACS Appl. Mater. Interfaces 2015, 7, 4381−4389

(36) Li, X. L.; Zhu, L. P.; Xu, Y. Y.; Yi, Z.; Zhu, B. K. A Novel Positively Charged Nanofiltration Membrane Prepared from N, N-Dimethylaminoethyl Methacrylate by Quaternization Cross-Linking. *J. Membr. Sci.* **2011**, *374*, 33−42.
(37) Stankovich, S.; Dikin, D. A.; Piner, R. D.; Kohlhaas, K. A.; Kleinhammes, A.; Jia, Y.; Wu, Y.; Nguyen, S. T.; Ruoff, R. S. Synthesis of Graphene-Based Nanosheets via Chemical Reduction of Exfoliated Graphite Oxide. *Carbon* **2007**, *45*, 1558−1565.
(38) Karim, Z.; Mathew, A. P.; Grahn, M.; Mouzon, J.; Oksman, K. Nanoporous Membranes with Cellulose Nanocrystals as Functional Entity in Chitosan: Removal of Dyes from Water. *Carbohydr. Polym.* **2014**, *112*, 668−676.
(39) Schaep, J.; Bruggen, B. V. d.; Vandecasteele, C.; Wilms, D. Influence of ion size and charge in nanofiltration. *Sep. Purif. Technol.* **1998**, *14*, 155−162.
(40) Peeters, J. M. M.; Boom, J. P.; Mulder, M. H. V.; Strathmann, H. Retention measurements of nanofltration membranes with electrolyte solutions. *J. Membr. Sci.* **1998**, *145*, 199−209.
(41) Kotov, N.; Haraszti, T.; Turi, L.; Zavala, G.; Geer, R.; Dekany, I.; Fendler, J. Mechanism of Defect Formation in the Self-assembly of Polymeric Polycation-Montmorillonite Ultrathin Films. *J. Am. Chem. Soc.* **1997**, *119*, 6821−6832.
(42) Nair, R.; Wu, H.; Jayaram, P.; Grigorieva, I.; Geim, A. Unimpeded Permeation of Water through Helium-leak−tight Graphene-based Membranes. *Science* **2012**, *335*, 442−444.
(43) Boukhvalov, D. W.; Katsnelson, M. I.; Son, Y.-W. Origin of Anomalous Water Permeation through Graphene Oxide Membrane. *Nano Lett.* **2013**, *13*, 3930−3935.
(44) Joshi, R.; Carbone, P.; Wang, F.; Kravets, V.; Su, Y.; Grigorieva, I.; Wu, H.; Geim, A.; Nair, R. Precise and Ultrafast Molecular Sieving through Graphene Oxide Membranes. *Science* **2014**, *343*, 752−754.

DOI: 10.1021/am508903g
ACS Appl. Mater. Interfaces 2015, 7, 4381−4389